Equation-of-state properties of high-energy-density matter using intense heavy ion beams with an annular focal spot

N. A. Tahir, D. H. H. Hoffmann, and A. Kozyreva
Institut für Kernphysik, Technische Universität Darmstadt, Schlossgarten Strasse 9, D-64289 Darmstadt, Germany

A. Shutov
Institute for Chemical Physics Research, Chernogolovka, Russia

J. A. Maruhn
Institut für Theoretische Physik, Universität Frankfurt, D-60054 Frankfurt, Germany

U. Neuner, A. Tauschwitz, P. Spiller, and R. Bock
Gesellschaft für Schwerionenforschung, Planckstrasse 1, D-64291 Darmstadt, Germany
(Received 17 December 1999)

This paper presents two-dimensional numerical simulations of the hydrodynamic response of solid as well as hollow cylindrical targets made of lead that are irradiated by an intense beam of uranium ions which has an annular focal spot. Using a particle tracking computer code, it has been shown that a plasma lens can generate such a beam with parameters used in the calculations presented in this paper. The total number of particles in the beam is 2×10^{11} and the particle energy is about 200 MeV/u that means a total energy of approximately 1.5 kJ. This energy is delivered in a pulse that is 50 ns long. These beam parameters lead to a specific energy deposition of 50–100 kJ/g and a specific power deposition of 1–2 TW/g in solid matter. These calculations show that in case of the solid lead cylinder, it may be possible to achieve more than 4 times solid lead density along the cylinder axis at the time of maximum compression. The pressure in the compressed region is about 20 Mbar and the temperature is a few eV. In the case of a hollow cylinder, one also achieves the same degree of compression but now the temperature in the compressed region is much higher (over 10 eV). Such samples of highly compressed matter can be used to study the equation-of-state properties of high-energy-density matter. It is expected that by the end of the year 2001, after completion of the upgrade of the existing facilities, the above beam parameters will be available at the Gesellschaft für Schwerionenforschung (GSI), Darmstadt. This will open up the possibility to carry out very interesting experiments on a number of important problems including the investigation of the EOS of high-energy-density matter.

PACS number(s): 51.50.+v, 51.60.+a, 51.70.+f

I. INTRODUCTION

The heavy ion synchrotron facility (SIS) at the Gesellschaft für Schwerionenforschung (GSI) Darmstadt is a unique facility that delivers intense beams of energetic heavy ions. The new high current injector [1] that consists of an RFQ (radio frequency quadrupole) and IH (interdigital H mode) structures has just become operational. The total number of 300 MeV/u Ar^{+10} ions that has been achieved in a single bunch is 3.2×10^{10} and the pulse length is of the order of 300 ns. It is expected that further optimization of accelerator parameters would increase the total number of particles in the beam to about 10^{11}. Later, the SIS will provide an intense beam of U^{+28} ions with a particle energy of about 200 MeV/u. Employment of a multiturn injection scheme that increases the beam current by a factor of 15 without any significant losses will allow a total number of 2×10^{11} uranium particles in the beam. Due to bunch compression performed by a powerful rf buncher, the pulse duration will be reduced to 50 ns. The total energy carried by the beam will be about 1.5 kJ. The beam intensity in the SIS will increase gradually over the next two years and the maximum design parameters of the upgrade will be achieved by the end of the year 2001. For further details about this scheme see Refs. [2,3].

The beam generated at the upgraded SIS facility will deposit a specific energy of 50–100 kJ/g and a specific power of 1–2 TW/g in solid matter. This will not only make it possible to study problems like energy loss of heavy ions in hot dense matter [4–16], but will also provide samples of high-energy-density matter. These samples of matter can be used to study the equation-of-state (EOS) properties of matter under extreme conditions [17–19].

Another very novel experiment that would be carried out at this facility is to study the possibility of creating metallic hydrogen [20–22] by imploding appropriately designed multilayered targets that contain a layer of frozen hydrogen or deuterium [23].

Numerical simulations are an essential tool to optimize the design of a future experiment, efficiently and economically. Use of sophisticated numerical simulation codes that include good models for the physical processes that are relevent to the experiment, can predict the experimental results with a reasonable accuracy. This could be very helpful in designing suitable diagnostic techniques to analyze the experiment.

Previously [24,25] we reported numerical simulations of the hydrodynamic response of a solid lead cylinder whose one face was irradiated by a heavy ion beam having same

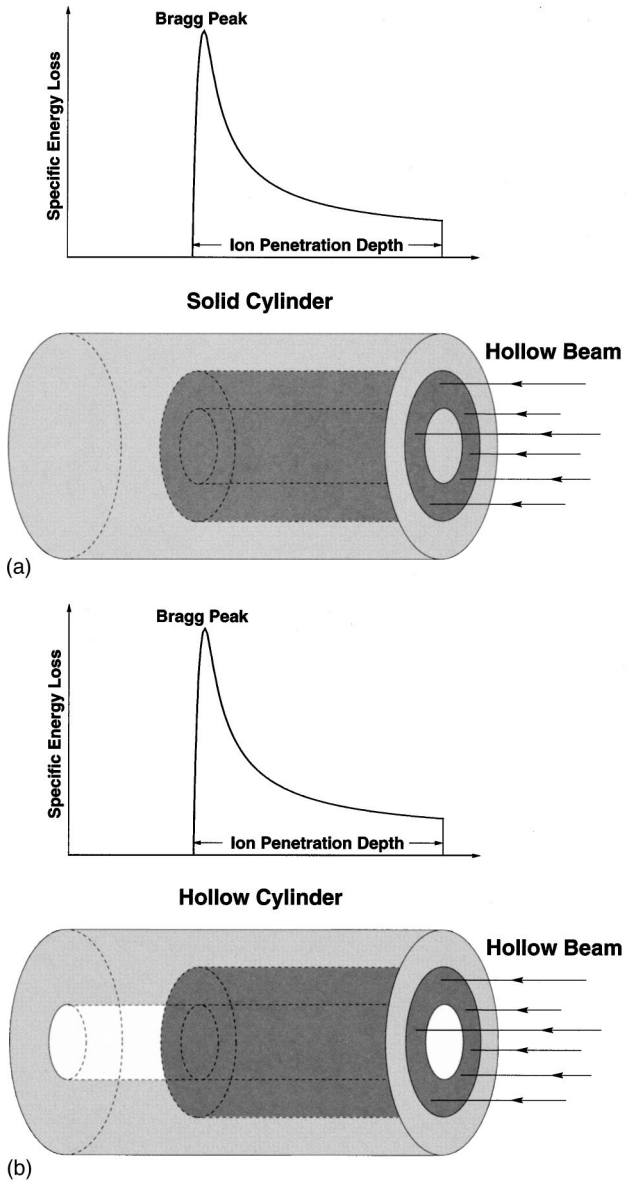

FIG. 1. (a) A ''super range'' solid cylindrical lead target irradiated by an intense heavy ion beam having an annular focal spot. (b) A ''super range'' hollow cylindrical lead target irradiated by an intense heavy ion beam having an annular focal spot.

parameters as the upgraded SIS beam. In these calculations we assumed that the beam had a circular spot with a radius r_b that was significantly less than the target radius r_c, and the cylinder length was smaller than the penetration depth of the projectile ions. The Bragg peak therefore lies outside the target and the specific energy deposition along the particle trajectory inside the target is fairly uniform. The inner part of the target material with a radius r_b, is strongly heated by the beam and the pressure in this heated zone increases substantially. This increase in pressure launches an outward going shock wave along the target radius. This can be approximated as a one-dimensional shock wave propagation in the radial direction and a one-dimensional computer code such as MEDUSA-KAT [26] could be used to treat this problem. The validity of this approximation in case of such a beam-target arrangement has been confirmed by using a two-dimensional computer code MULTI2D [27].

TABLE I. Geometrical, beam, and field parameters suitable for generation of a beam with an annular spot.

Geometry parameters	Plasma lens length	0.1 m
	Lens radius	0.01 m
	Distance to profile plane	0.085 m
Beam parameters	Magnetic rigidity	5.7 T m
	dp/p	$\pm 1\%$
	ϵ_x/y	5 mm mrad
	α_x/y	0
	β_x/y	20 m
Field coefficients	k_1	310 T/m
	k_2	11000 T/m^2
Emittance growth	$E_{\mathrm{rms},i}/E_{\mathrm{rms},f}$	4.9

The above beam-target arrangement simplifies the problem significantly, but a substantial part of the beam energy cannot be utilized and as a result the specific power deposition in the target remains low. This in turn leads to lower compression of the target material. In order to make use of the total beam energy, one needs to design a ''super range'' target whose length is larger than the beam penetration depth. The Bragg peak now lies inside the target and the specific energy deposition is no longer uniform along the particle trajectory. One therefore cannot use a one-dimensional computer program to treat this problem. Instead, it is necessary to employ a two-dimensional code to simulate such an experiment.

In a previous paper we reported [28] two-dimensional numerical simulations of the hydrodynamic behavior of a ''super range'' solid lead target that was irradiated by the beam that will be generated at the upgraded SIS facility. These simulations were carried out using a two-dimensional computer code BIG2 [29]. In these calculations we assumed a normal beam with a circular beam spot and the beam deposition profile was Gaussian in the radial direction. The full width at half maximum (FWHM) of the distribution was considered to be 1 mm which could be regarded as the effective beam radius. The material that lies within the cylinder whose length is equal to the penetration depth of the projectile ions and whose radius is equal to the beam radius, is strongly heated due to the energy deposited by the beam in this region. The pressure in this hot zone increases substantially (to a few Mbar) that drives an outgoing shock wave along the radial direction as well as in the beam direction. In these simulations we achieved a maximum temperature of about 13 eV and a corresponding pressure of about 3.5 Mbar in the Bragg peak region. In the shock compressed region on the other hand, the maximum density was about 22 g/cm^3 which is a factor 2 higher than the solid lead density, while the temperature was of the order of 1 eV and the pressure was of the order of 3 Mbar. This region represents high density, high pressure, but relatively low temperature matter which is very interesting for investigation of the EOS of matter in the regime of nonideal plasmas.

The degree of compression could be significantly increased if one irradiates a solid cylindrical target with a beam that has an annular focal spot [see Fig. 1(a)]. In this case a ring of hot material is created by the beam in the cylinder and the dimensions of this hot zone are determined by the

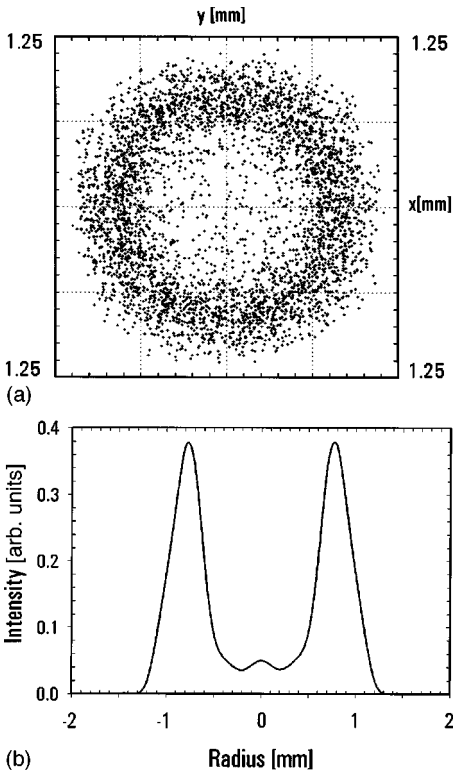

FIG. 2. (a) Calculated particle distribution before the first order focal plane of the plasma lens, (b) corresponding beam crossection.

dimensions of the beam focal spot and the ion range. A cylinder of solid cold material is enclosed in the hot zone and also the hot zone is followed by a shell of solid cold material. The very high pressure in the ring of hot material launches shock waves in the radial direction, inwards as well as outwards and also a shock propagates along the cylinder length ahead of the Bragg peak. The inmoving shock wave gets stronger and stronger as it converges towards the cylinder axis that results in a much higher density when the shock wave arrives at the axis [30]. The outgoing shock wave in the radial direction as well as that along the target length weakens as it moves outwards because of this geometrical effect. In our simulations we find that a maximum density of more than four times the solid lead density is achieved at the cylinder axis at the time of maximum compression.

If, on the other hand, one uses a hollow cylinder that is irradiated by a beam with an annular focal spot [see Fig. 1(b)], one will not only achieve a high density and high pressure along the target axis, but one will also achieve a high temperature in the compressed region. This is because when the target is heated, the inner boundary moves inwards and when it collapses at the cylinder axis, the kinetic energy that is stored in this moving part of the target is converted into thermal energy. These simulation results show that using appropriate beam-target geometry, the upgraded SIS beam will be capable of creating samples of high-energy-density matter that can be used to study equation-of-state properties of important materials under such extreme conditions.

We acknowledge that important experimental work has already been done on measurement of the EOS properties of high-energy-density matter using high power lasers [31–33], but ion-beam generated plasmas have a number of very unique features as compared to laser-produced plasmas, as

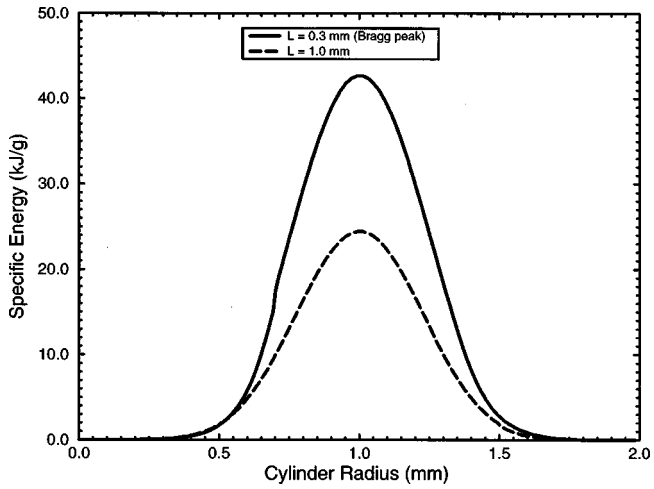

FIG. 3. Specific energy deposition vs target radius at $t=50$ ns, at $L=0.3$ mm (Bragg peak), and 1.0 mm, respectively, annular beam focal spot, inner radius$=0.50$ mm, outer radius$=1.50$ mm, Gaussian power deposition in radial direction, 200 MeV/u uranium ions, $N=2\times10^{11}$, $\tau=50$ ns, parabolic power profile in time, cold range of projectile ions in solid lead$=1.7$ mm, Bragg peak lies at $L=0.3$ mm.

discussed in detail in Ref. [28]. This makes the planned ion-beam-matter interaction experiments at the GSI very important.

In Sec. II we discuss how one can produce a heavy ion beam that has an annular focal spot while in Sec. III we describe important range energy relations and beam-target parameters. The simulation results are presented in Sec. IV and conclusions drawn from this work are noted in Sec. V.

II. GENERATION OF INTENSE HEAVY ION BEAMS WITH AN ANNULAR FOCAL SPOT

Beams with a ring type focal spot can be generated using a magnetic flux density that is nonlinear in radial direction. A plasma lens [34] is therefore a very suitable device to create such beams as the flux density in this device is axisymmetric by nature. Although in normal operation a plasma lens has linear focusing properties, there is a phase in which the discharge current in the lens is nonuniform [35].

In order to estimate the ion optical properties of such a nonlinear flux density distribution, we have employed a particle tracking computer code. This code transforms single particles of an initial KV distribution (uniformly filled phase space area) through the plasma lens and the following drift space. The magnetic field is purely azimuthal with sharp edges along the axis. The radial dependence of the magnetic flux density distribution can be written as a Taylor expansion

$$B(r)=k_1r+k_2r^2+k_3r^3+\cdots, \tag{1}$$

where k_1 denotes the linear part of the field, k_2 denotes the second order term, and k_3 represents the third order term. The units of these coefficients are given as $k_1=T/m$, $k_2=T/m^2$, $k_3=T/m^3$, and so on. In the specific case that we consider in this paper, only first and second order terms are important and all the higher order terms are zero.

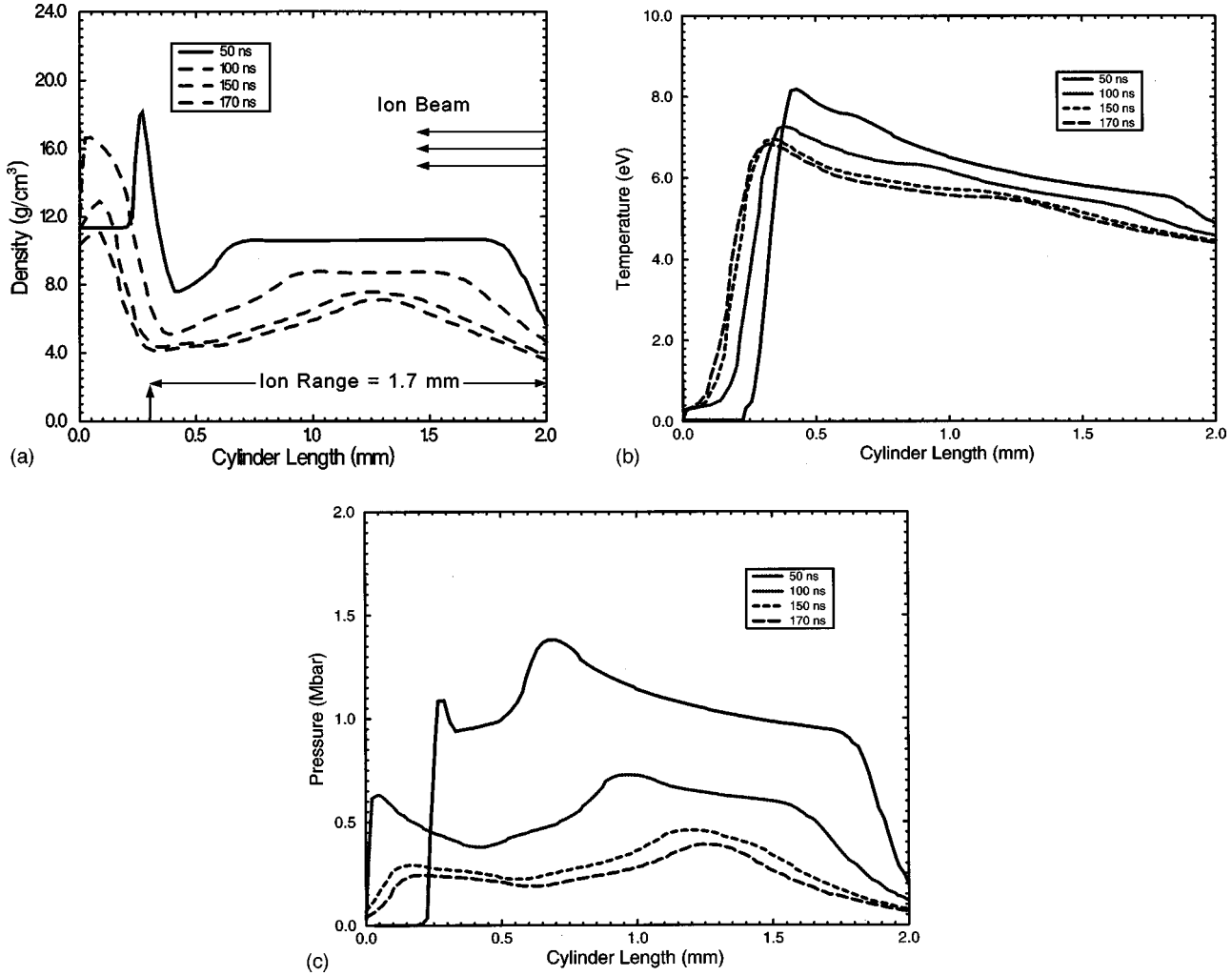

FIG. 4. (a) Density, (b) temperature, and (c) pressure vs cylinder length at $r=1.0$ mm at different times [case of Fig. 1(a)].

The distance of the profile plane where the particle distribution is being calculated is located at small distance from the first order focal plane in the direction of the lens. In the example shown in Table I, it is assumed that the beam radius

$$R_{x/y}=\sqrt{\beta_{x/y}\epsilon}$$

is matched to the plasma lens radius. The beam envelope has a waist with $\alpha=0$ at the entrance of the plasma lens. α and β are known as Twiss parameters describing the shape and inclination of the emittance area in the transverse phase space. The transverse rms emittance of the beam ϵ_{rms} is determined from the particle trajectories in the profile plane. By comparing the final emittance $\epsilon_{\mathrm{rms},f}$ with the initial emittance $\epsilon_{\mathrm{rms},i}$ the emittance growth factor by the nonlinear field components can be determined. The relation between the emittance of the initially defined KV distribution and the rms emittance is $\epsilon_{\mathrm{KV}}=4.\epsilon_{\mathrm{rms}}$. Furthermore, a parabolic longitudinal momentum spread of $\pm 1\%$ is assumed. This momentum spread will be caused in the experiments as a result of strong longitudinal compression. The space charge effects as well as higher order aberrations of the beam guiding elements between the accelerator and the plasma lens were not considered. The dispersion function in the plasma lens is assumed to be zero, otherwise the beam size in the horizontal plane that is dependent on the product of the dispersion function and the momentum spread, would grow. A typical parameter regime is presented in Table I.

Using the parameters given in the table, we generated a beam with a ring type focal spot and the radii of this ring have submillimeter dimensions. Figure 2(a) shows the particle distribution in the profile plane while Fig. 2(b) presents the corresponding cross section.

III. RANGE-ENERGY RELATIONS AND BEAM-TARGET PARAMETERS

A. Range-energy relations

In the case of ion-beam matter interaction studies, one of the most important parameters that determines the maximum achievable temperature in the target is the specific power deposition P_s. This parameter is defined as follows:

$$P_s=\frac{E_s}{\tau}, \tag{2}$$

where τ is the pulse duration and E_s is the specific energy deposition given by

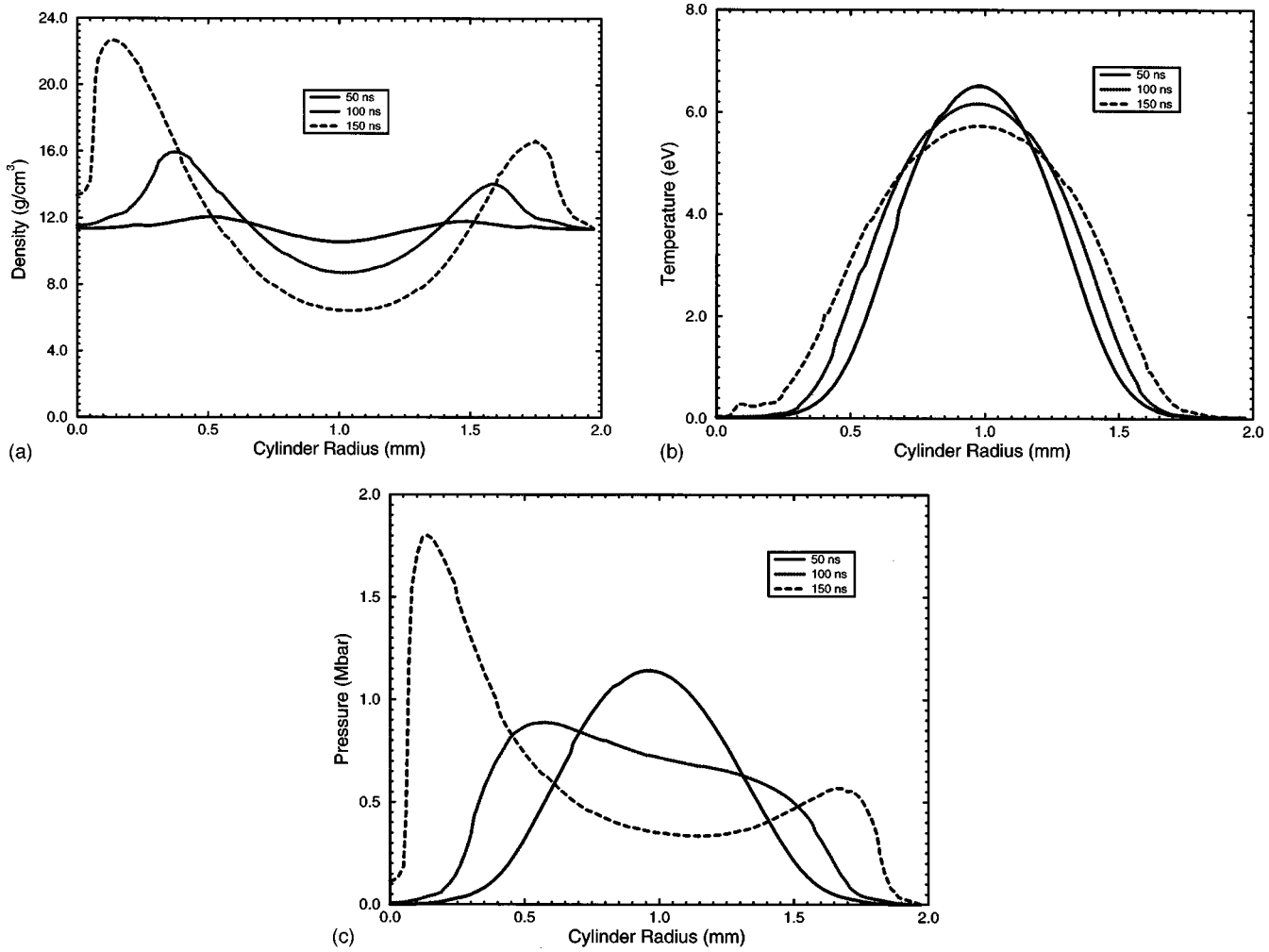

FIG. 5. (a) Density, (b) temperature, and (c) pressure vs cylinder radius at $L=1.0$ mm (Bragg peak lies at $L=0.3$ mm) at different times [case of Fig. 1(a)].

$$E_s=\frac{(1/\rho)(dE/dx)N}{\pi r_b^2}. \tag{3}$$

In the above equation, $(1/\rho)(dE/dx)$ is the specific energy loss due to a single ion, ρ is the target material density, x is the coordinate along the particle trajectory, N is the total number of particles in the beam, and r_b is the beam radius.

Previous numerical simulations [24,25,28] show that the temperature achieved in a solid lead target that is irradiated with the future SIS beam is of the order of 10 eV. Therefore, for the purpose of calculating $(1/\rho)(dE/dx)$, one may regard the target material to be cold and the TRIM code [36] could be used to perform these calculations.

B. Beam-target parameters for the case of solid cylinder irradiated by a beam with an annular focal spot

The beam-target geometry for this type of experiment is shown in Fig. 1(a). In our calculations we used a solid lead cylinder having a radius as well as a length of 2.0 mm. According to the TRIM code [36], the range of the 200 MeV/u uranium ions in solid lead is about 1.7 mm and therefore the ions are completely stopped in the target.

We assume that the total number of ions in the beam, $N=2\times10^{11}$ and the pulse duration, $\tau=50$ ns. The beam power deposition profile in the radial direction is considered to be Gaussian given by

$$P(r)=P_0\exp\left[-\frac{(r-\mu)^2}{2\sigma^2}\right], \tag{4}$$

where μ is mean deviation and σ is standard deviation of the distribution. The above Gaussian distribution represents the power deposition profile along the radial direction in a hollow beam.

It has been shown in Sec. II that using a plasma lens one can generate such a hollow ion beam whose ring shaped focal spot has sub-millimeter radii. In our calculations we assume somewhat more pessimistic parameters that lead to larger spot radii than determined by these calculations. We assume a $\mu=1.0$ mm and a $\sigma=0.2128$ mm This value of σ correspond to a FWHM=0.5 mm. The time profile of the beam power is assumed to be parabolic given by

$$P(t)=-\frac{6E}{\tau^3}[t^2-\tau t], \tag{5}$$

where E is the total energy in the beam and in this case is about 1.5×10^3 J.

C. Beam-target parameters for the case of hollow cylinder irradiated by a beam with an annular focal spot

The beam-target geometry for this type of experiments is shown in Fig. 1(b). We consider a hollow cylinder that has an inner radius=0.5 mm, an outer radius=2.5 mm, and a length=3.0 mm.

The inner radius of the beam spot ring is also assumed to be 0.5 mm while its outer radius is taken to be 1.5 mm and the beam deposition profile is considered to be parabolic in the radial direction. The rest of the beam parameters are assumed to be same as in the previous case.

IV. NUMERICAL SIMULATIONS RESULTS

In this section we present our numerical simulation results that have been obtained using a one temperature, two-dimensional hydrodynamic simulation model BIG2 [29]. This code uses an arbitrary Lagrangian-Eulerian (ALE) method that combines both the Lagrangian and the Eulerian approaches. It is based on a Gudonov type scheme and has a second order accuracy in space for solving hydrodynamic equations. It uses a rectangular grid and uses a sophisticated EOS data described elsewhere [37]. The code includes the electron thermal conduction, although this energy transport mechanism does not play any important role under the physical conditions considered in this problem. The code also includes energy deposition of the incident ions taking into account the beam geometry.

A. Solid cylinder irradiated by a uranium beam with an annular focal spot

As seen from Fig. 1(a), the beam is incident on the right face of the cylindrical target. The range of 200 MeV/u uranium ions in solid cold lead is about 1.7 mm [36]. The ions therefore penetrate 1.7 mm into the target through the right face that is located at $L=2.0$ mm and the Bragg peak lies at the end of the range at $L=0.3$ mm.

The ion energy is deposited in a cylindrical ring with a length 1.7 mm, an inner radius 0.50 mm, and an outer radius of 1.50 mm. The Bragg peak lies at length $L=0.3$ mm while the maxima of the Gaussian power deposition profile occurs at a radius $r=1.0$ mm. The highest value of the specific energy deposition therefore occurs at the point $L=0.3$ mm, $r=1.0$ mm. This is clearly seen from Fig. 3 where we plot the specific energy deposition along the target radius at two points along the cylinder length, namely, at $L=0.3$ mm (that is 1.7 mm to the left of the right face of the target and where the Bragg peak lies) and $L=1.0$ mm (that lies 1.0 mm to the left of the right face of the cylinder and is before the Bragg peak), respectively. Also this figure is plotted at time, $t=50$ ns when the beam has just delivered its total energy.

The high pressure in the hot zone launches shock waves along radial direction (inwards as well as outwards) and along the length. The inmoving shock wave becomes stronger and stronger as it converges towards the cylinder axis, while the outgoing shock waves in the radial as well as axial directions become weaker due to the cylindrical geometry of the problem. The shock converges at the axis at $t=165$ ns.

To study the behavior of these shock waves in a more quantitative manner, we present in Fig. 4(a) the density profiles along the cylinder length at $r=1.0$ mm at four different times, namely 50, 100, 150, and 170 ns, respectively. The ions are incident on the right face of the cylinder and they penetrate 1.7 mm along the cylinder length. The pressure is the highest in the Bragg peak region that launches a shock wave towards the left face of the target in the beam direction. It is seen that the maximum density in the shock region at $t=50$ ns is about 18 g/cm^3 while in the Bragg peak region the density has become significantly lower. The shock arrives at the outer boundary (left face of the cylinder) at about 100 ns and the latter two profiles show the expansion along the beam direction.

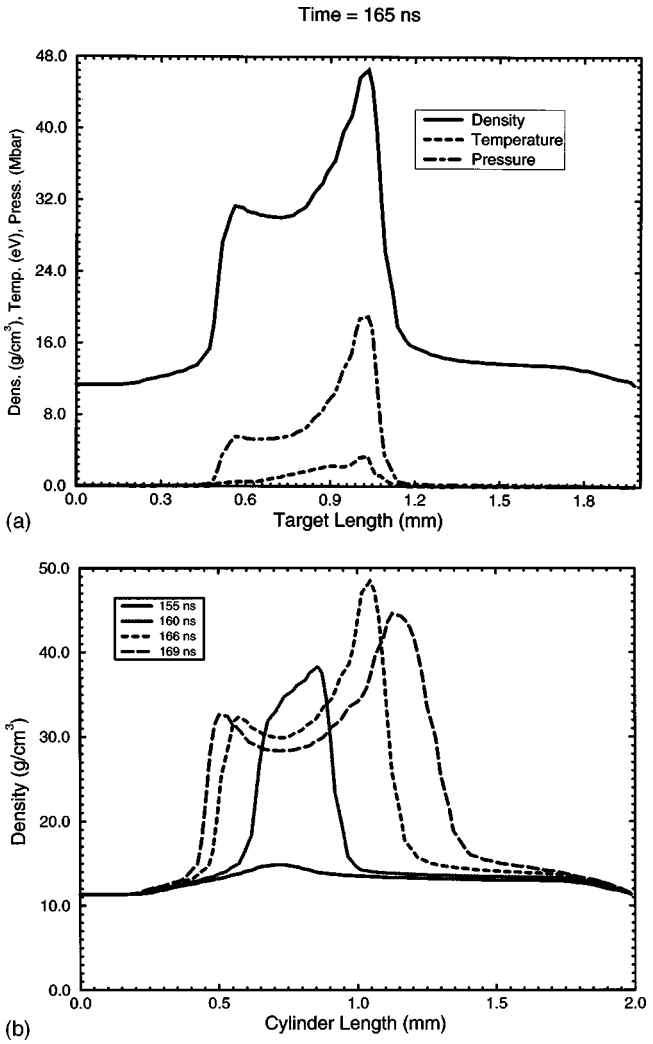

FIG. 6. (a) Density, temperature, and pressure vs cylinder length at $r=0.0$ mm (on axis) at $t=165$ ns (maximum compression). (b) Density vs length at $r=0.0$ mm at different times.

The corresponding temperature and pressure profiles are shown in Figs. 4(b) and 4(c), respectively. Figure 4(b) shows that the maximum temperature in the Bragg peak region at $t=50$ ns is of the order of 8 eV whereas the pressure profile in Fig. 4(c) shows a double peak behavior. The main pressure peak that lies to the right of the Bragg peak shows a pressure of 1.3 Mbar. This region has a solid density and a relatively high temperature (about 7 eV). The second smaller pressure peak lies to the left of the Bragg peak and it has a value of 1.1 Mbar. The density in this region is about 18 g/cm^3 while the temperature is much less than 1 eV. In the

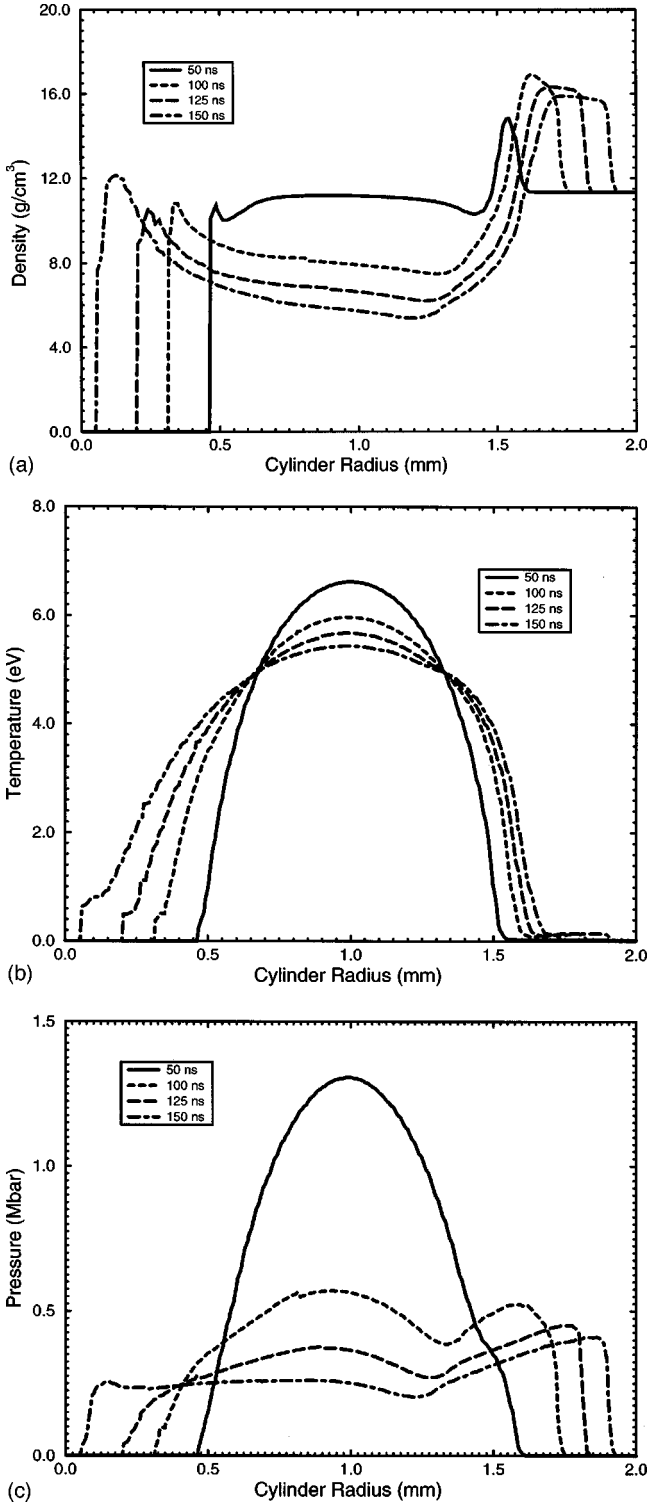

FIG. 7. (a) Density, (b) temperature, and (c) pressure vs cylinder radius at $L=1.8$ mm (Bragg peak lies at $L=1.3$ mm) at different times [case of Fig. 1(b)].

Bragg peak region, on the other hand, the density is significantly lower than the solid density and the temperature is about 8 eV while the pressure is just about 1 Mbar. This therefore provides one with three different regimes of high-energy density matter for EOS investigations. To the right of the Bragg peak, one has a high pressure, solid density, and high temperature region. In the Bragg peak one has a low density, high temperature and high pressure region. To the left of the Bragg peak, one has a supersolid density, high pressure but low temperature region that represents the interesting regime of nonideal plasmas. All these three regimes are very important and one should be able to investigate the EOS properties of matter in these different states.

It is also of interest to study the behavior of the target along the radial direction. In Figs. 5(a), 5(b), and 5(c), respectively, we plot the density, temperature, and pressure along the cylinder radius at $L=1$ mm at three different values of time. It is seen from Fig. 5(a) that at $t=50$ ns, when the beam has just delivered its total energy, the density has decreased at $r=1$ mm which is the position where maximum of the Gaussian deposition distribution lies and the highest energy deposition occurs. Across this position, on both sides, the density has increased that shows the development of shock waves in the radial direction inwards as well as outwards. The corresponding curves in Figs. 5(b) and 5(c) again show a Gaussian behavior of the temperature and pressure along the radial direction with the maxima lying at $r=1$ mm. This pressure profile is responsible for driving the shock waves in the radial direction. Further development of the shock waves is shown by the curves plotted at 100 and 150 ns and it is clearly seen that the inmoving shock is being amplified.

The shock converges at this point on the axis ($L=1$ mm) at $t=165$ ns and the maximum compression occurs. In Fig. 6(a) we plot the density, temperature, and pressure along the length at $r=0.0$ (along the cylinder axis) at $t=165$ ns. It is seen that one gets a very high compression and a maximum density of about 47 g/cm^3 is acvieved which is more than 4 times solid lead density. The maximum pressure is about 19 Mbar while the temperature is about 3 eV.

It is to be noted that the energy deposition is not uniform along the particle trajectory and correspondingly, the pressure profile generated by this deposition is also nonuniform. The pressure is highest in the Bragg peak region and it decreases as one moves towards the right face of the cylinder, in opposite direction to the particle trajectory. Also the maximum of the pressure profile along the cylinder length occurs at $r=1.0$ mm, where the maxima of the Gaussian distribution lies. Due to the nonuniformity of pressure, the inmoving shock wave in radial direction arrives at the axis at different times along different points on the axis. This is demonstrated in Fig. 6(b) where we plot the target density vs length at different times. It is seen that the maximum density is achieved at $t=165$ ns at $L=1.0$ mm and this highly compressed region expands along the axis with time, while the density decreases. The density in the compressed region remains above 30 g/cm^3 between 160 and 190 ns, which provides a time of about 30 ns for experimental investigations.

B. Hollow cylinder irradiated by a uranium beam with an annular focal spot

Figure 2(b) shows the beam-target arrangement for an experiment that involves compression of a hollow cylinder which is irradiated by an ion beam having an annular focal spot. The target is made of lead and the beam is incident on the right face of the target. It is assumed that the inner radius of the cylinder as well as that of the annular beam focal spot is 0.5 mm. The outer radius of the target is 2.5 mm while that

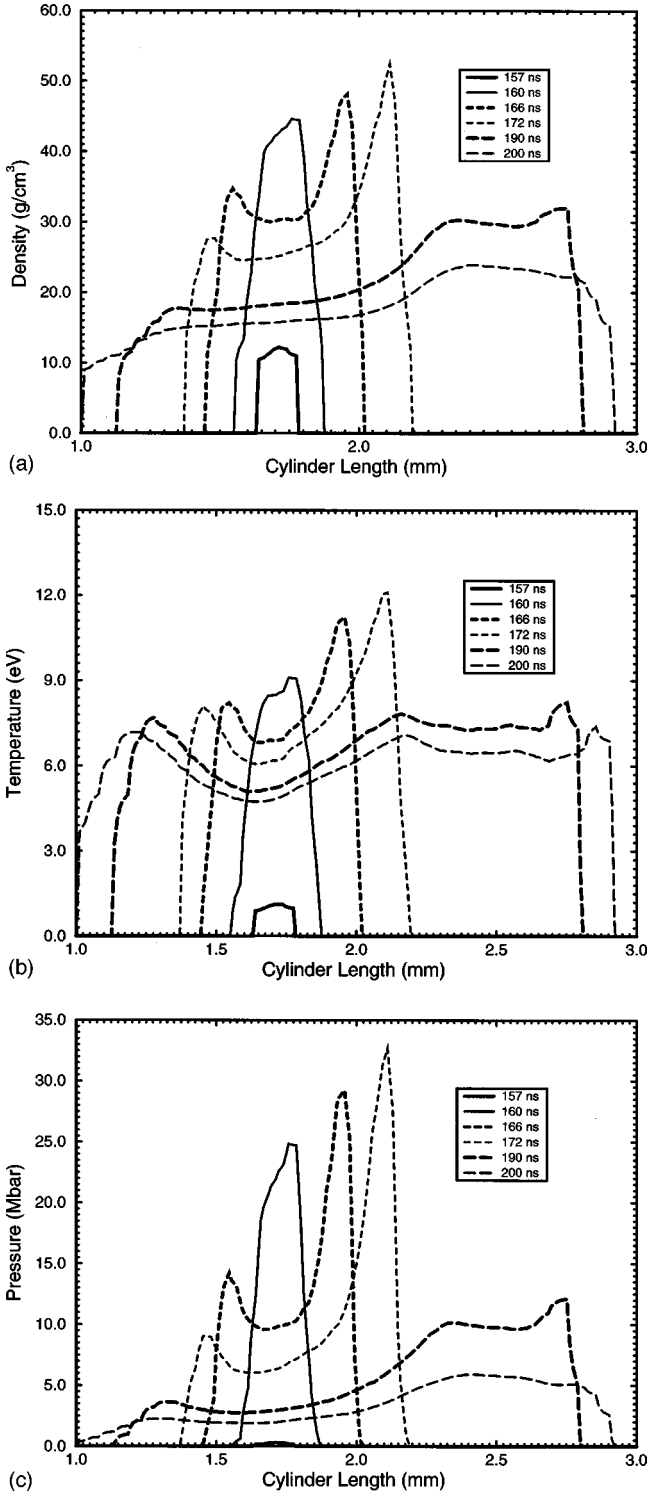

FIG. 8. (a) Density, (b) temperature, and (c) pressure vs cylinder length at $r = 0.0$ mm (on axis) at different times.

of the beam focal spot is 1.5 mm. The beam deposition profile is parabolic in the radial direction. The length of the target is 3.0 mm.

The ions penetrate about 1.7 mm along the cylinder length and a hollow cylinder of very hot and high pressure material is created inside the target. The length of this hot hollow cylindrical region is 1.7 mm, inner radius is 0.5 mm, and outer radius is 1.5 mm. This hot zone is surrounded by a

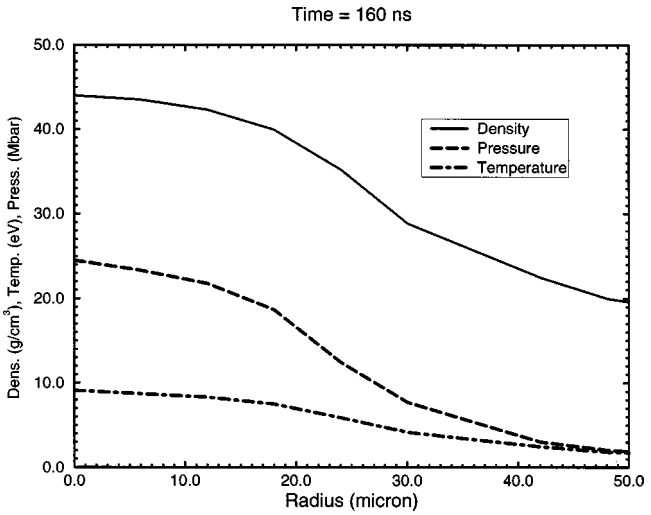

FIG. 9. Density, temperature and pressure vs cylinder radius at $L = 7$–8 mm, at $t = 160$ ns.

solid cold shell that has an outer radius of 2.5 mm. Also to the left of the Bragg peak, between $L = 0$ and 1.3 mm, there is solid cold lead. The very high pressure in the hot region launches shock waves along the cylinder length as well as along the radius in outward direction. However since the cylinder is hollow, no shock wave propagates inwards along the radial direction. Instead, a rarefaction wave moves in and the inner surface of the hot hollow cylindrical region expands towards the axis.

In Fig. 7(a) we plot the target density along the cylinder radius at $L = 1.8$ mm at four different points in time. It is seen that a shock wave propagates outward in the radial direction and the position of the inner cylinder boundary moves as the inner surface of the cylinder expands. It is interesting to note that there is a very sharp gradient of the density across the inner boundary and there is a density peak at the position of the inner boundary. This is because the radius of the beam is fixed. As the material is heated due to energy deposition, it expands and moves out of the beam spot region. The material that moves out of the beam spot region during the early stages remains relatively cold and dense as it moves towards the cylinder axis. The curve at $t = 150$ ns shows that the inner cylinder surface has moved very close to the position $r = 0.0$ mm and the density at the center has started to increase as the material collapses. The temperature and pressure curves corresponding to Fig. 7(a) are plotted in Figs. 7(b) and 7(c), respectively.

It is to be noted that the energy deposition and hence the pressure profile along the target length is not uniform. As a result of this the velocity with which the inner cylinder surface moves inwards is also not uniform. It increases as one moves along the particle trajectory in the beam direction. Therefore the entire inner target surface does not converge at the axis simultaneously, but different parts arrive at the axis at different times depending on their corresponding velocities. In Fig. 8(a) we plot the density along the target length at $r = 0.0$ (axis) at six different times. It is seen that at $t = 157$ ns, the density starts to increase around $L = 1.75$ mm. Since the cylinder is 3.0 mm long and the beam is incident on its right face, the ions will penetrate along the cylinder length up to a distance 1.7 mm that means that the Bragg

TABLE II. Achievable compression in different beam-target geometries.

Beam-target configuration	Density (g/cm^3)	Temperature (eV)	Pressure (Mbar)
Solid lead cylinder and annular beam spot	48.0	3.0	20.0
Hollow lead cylinder and annular beam spot	57.0	13.0	33.0

peak will lie at $L=1.3$ mm on the X axis of Fig. 8(a). Since the energy deposition has its highest value in the Bragg peak region, the higher pressure in this region pushes material to the left and to the right that results in a reduced density in the Bragg peak region itself. Therefore we do not see any density peak on the axis exactly below the Bragg peak but it occurs to the right of the Bragg peak at $L=1.75$ mm.

The corresponding temperature and pressure profiles are shown in Figs. 8(b) and 8(c), respectively. Due to the high pressure in the highly compressed region, the material is pushed to the right as well as to the left of the compressed region and this region expands with time. In addition to that, more material continues to arrive on the axis along the cylinder length from above. At $t=172$ ns, we achieve a maximum density of about 55 g/cm^3, a temperature of 13 eV and a pressure of about 33 Mbar at $L=2.2$ mm. The later two curves show the expansion of the target along its length.

We also note that unlike the previous case of irradiation of a solid cylinder with an annular beam, in the present calculations, not only we achieve a high density and high pressure, but we also achieve a high temperature. This is because in the present case the material is set in motion due to the rarefaction wave and a significant amount of kinetic energy is stored in the target. When this moving material collapses at the target axis, all the kinetic energy is instantaneously converted into thermal energy that results at a high temperature.

In Fig. 9 we plot the density, temperature and pressure along cylinder radius at $L=1.80$ mm at $t=160$ ns. It is seen that the radius of the highly compressed region is a few tens of microns.

V. SUMMARY AND CONCLUSIONS

This paper presents two-dimensional numerical simulations of the hydrodynamic response of solid as well as hollow lead cylindrical targets that are irradiated by an intense heavy ion beam which has an annular focal spot. The total number of particles in the beam is 2×10^{11} and the particle energy is on the order of 200 MeV/u that means 1.5 kJ total energy in the pulse. The pulse is delivered in 50 ns and the beam power profile in time is parabolic. These beam parameters will be available at the upgraded GSI synchrotron facility by the end of the year 2001.

Our calculations show that in case of the solid cylinder, one can achieve a compression of over 4 times solid lead density, a pressure of about 20 Mbar and a temperature of a few eV along the cylinder axis at the time of maximum compression. In case of the hollow cylinder, one would achieve a compression of about 5 times solid lead density, a pressure of about 30 Mbar and a temperature of over 10 eV. These results are summarized in Table II. Such samples of high-energy-density matter will be created at the upgraded SIS facility and equation-of-state properties of matter under such extreme conditions will be investigated experimentally.

ACKNOWLEDGMENT

The authors wish to thank the German Ministry of Research and Development (BMBF) for providing financial support to carry out this work.

[1] U. Ratzinger (unpublished).
[2] R. W. Müller and P. Spiller (unpublished).
[3] K. Blasche, O. Boine-Frankheim, H. Eickoff, M. Emmerling, B. Franczak, I. Hofmann, K. Kaspar, U. Ratzinder, and P. Spiller (unpublished).
[4] D. H. H. Hoffmann, K. Weyrich, H. Wahl, D. Gardes, R. Bimbot, and C. Fleurier, Phys. Rev. A **42**, 2313 (1990).
[5] J. Jacoby *et al.*, Phys. Rev. Lett. **65**, 2007 (1990).
[6] E. Boggash, J. Jacoby, H. Wahl, K.-G. Dietrich, D. H. H. Hoffmann, W. Laux, M. Elfers, C. R. Haas, V. P. Dubenkov, and A. A. Golubev, Phys. Rev. Lett. **66**, 1705 (1991).
[7] K. G. Dietrich, D. H. H. Hoffmann, E. Boggash, J. Jacoby, H. Wahl, M. Elfers, C. R. Hass, and V. P. Dubenkov, Phys. Rev. Lett. **69**, 3623 (1992).
[8] S. Stöwe, R. Bock, M. Dornik, P. Spiller, M. Stetter, V. E. Fortov, V. Mintsev, M. Kulish, A. Shutov, V. Yakushev, B. Sharkov, A. Golubev, B. Bruynetkin, U. Funk, M. Geissel, D. H. H. Hoffmann, and N. A. Tahir, Nucl. Instrum. Methods Phys. Res. A **415**, 384 (1998).
[9] U. Funk, R. Bock, M. Dornik, M. Geissel, M. Stetter, S. Stöwe, N. A. Tahir, and D. H. H. Hoffmann, Nucl. Instrum. Methods Phys. Res. A **415**, 68 (1998).
[10] C. Stöckel, O. Boine-Frankheim, M. Geissel, M. Roth, H. Wetzler, W. Seelig, O. Iwase, P. Spiller, R. Bock, W. Süß, and D. H. H. Hoffmann, Nucl. Instrum. Methods Phys. Res. A **415**, 558 (1998).
[11] C. Deutsch and G. Maynard, Phys. Rev. A **26**, 665 (1982).
[12] T. Mehlhorn, J. Appl. Phys. **52**, 6522 (1981).
[13] E. Nardi and Z. Zinamon, Phys. Rev. Lett. **49**, 1251 (1982).
[14] R. O. Bangerter, J. W.-K. Mark, and A. R. Thiessen, Phys. Lett. **88A**, 225 (1982).
[15] C. Deutsch, Ann. Phys. (N.Y.) **11**, 1 (1986).
[16] K. A. Long and N. A. Tahir, Phys. Rev. A **35**, 2631 (1987).
[17] R. Redmer, Phys. Rev. E **59**, 1073 (1999).
[18] H. Kitamura and S. Ichimaru, J. Phys. Soc. Jpn. **65**, 1250 (1996).
[19] A. V. Bushman and V. Fortov, *Wide-Range Equation of State for Matter Under Extreme Conditions*, Vol. 1 of Soviet Tech-

nica Review B, Thermonuclear Physics (Harwood, London, 1987).
[20] W. J. Nellis, A. C. Mitchell, P. C. McCandless, D. J. Erskine, and S. T. Weier, Phys. Rev. Lett. **68**, 2937 (1992).
[21] S. T. Weir, A. C. Mitchell, and W. J. Nellis, Phys. Rev. Lett. **76**, 1860 (1996).
[22] H. K. Mao and R. J. Hemley, Rev. Mod. Phys. **66**, 671 (1994).
[23] N. A. Tahir, D. H. H. Hoffmann, J. A. Maruhn, K.-J. Lutz, and R. Bock, Phys. Lett. A **249**, 489 (1998).
[24] N. A. Tahir, D. H. H. Hoffmann, J. A. Maruhn, K.-J. Lutz, and R. Bock, Phys. Plasmas **5**, 4426 (1998).
[25] N. A. Tahir, D. H. H. Hoffmann, J. A. Maruhn, P. Spiller, and R. Bock, Phys. Rev. E **60**, 4715 (1999).
[26] N. A. Tahir, K. A. Long, and E. W. Laing, J. Appl. Phys. **60**, 898 (1986).
[27] R. Ramirez *et al.*, Laser Part. Beams **16**, 91 (1998).
[28] N. A. Tahir, D. H. H. Hoffmann, A. Kozyreva, A. Shutov, J. A. Maruhn, U. Neuner, A. Tauschwitz, P. Spiller, and R. Bock, Phys. Rev. E **61**, 1975 (2000).
[29] V. E. Fortov, B. Goel, C.-D. Munz, A. L. Ni, A. V. Shutov, and O. Yu. Vorobiev, Nucl. Sci. Eng. **123**, 169 (1996).
[30] Ya. B. Zel'Dovich and Yu. P. Raizer, *Physics of Shock Waves and High-Temperature Hydrodynamic Phenomena* (Academic, New York, 1967), Vols. I and II.
[31] B. Faral, R. Fabbro, J. Virmont, F. Cottet, J. P. Romain, and H. Repin, Phys. Fluids B **2**, 371 (1990).
[32] A. M. Evans, N. J. Freeman, P. Graham, C. J. Horsfield, S. D. Rorman, B. R. Thomas, and A. J. Tyrrell, Laser Part. Beams **14**, 113 (1996).
[33] R. Cauble, L. B. Da Silva, T. S. Perry, D. R. Bach, K. S. Budil, P. Celliers, G. W. Collins, A. Ng, T. W. Barbee, B. A. Hammel, N. C. Holmes, J. D. Kilkenny, R. J. Wallace, G. Chiu, and N. C. Woolsey, Phys. Plasmas **4**, 1857 (1997).
[34] M. Stetter, U. Neuner, S. Stöwe, M. Dornik, D. H. H. Hoffmann, R. Kowalewicz, P. Spiller, and A. Tauschwitz, Fusion Eng. Des. **32-33**, 503 (1996).
[35] A. Tauschwitz, Stromtragende Plasmalinse, Ph.D. thesis, Technical University of Darmstadt, 1993.
[36] J. F. Ziegler, J. P. Biersack, and U. Littmark, *The Stopping and Ranges of Ions in Solids* (Pergamon, New York, 1996).
[37] I. V. Lomonosov, A. V. Bushman, and V. E. Fortov, in *High-Pressure Science and Technology*, edited by S. C. Schmidt, J. W. Schaner, G. A. Samara, and M. Ross (AIP, New York, 1994), Pt. 1, p. 117.